JAPANESE JOURNAL OF APPLIED PHYSICS
VOL. 28, NO. 10, OCTOBER, 1989, pp. 1856-1863

Electron Mobility in Si Inversion Layers

Kazuo MASAKI, Chihiro HAMAGUCHI†, Kenji TANIGUCHI†
and Masao IWASE††

Anan College of Technology, Anan City, Tokushima 774
†Department of Electronic Engineering, Faculty of Engineering, Osaka University, Suita City, Osaka 565
††ULSI Research Center, Toshiba Corporation, 1 Komukai Toshiba-cho, Saiwai-ku, Kawasaki 210

(Received May 29, 1989; accepted for publication August 19, 1989)

Gate voltage dependence of electron mobility in n-channel MOSFETs is investigated using Hall effect and channel conductance measurements at room temperature and at 77 K. The electron mobilities obtained by the two different methods show a good agreement with each other and exhibit a decrease with increasing gate voltage in the region of high effective normal field. The theoretical model for electron mobility is given based on the interactions of two-dimensional electron gas confined in the inversion layer with acoustic phonons, intervalley phonons, surface-roughness and ionized impurities. An analytical expression is obtained for the electron mobility, where three types of f- and g-intervalley phonons are included. The calculated results show a good agreement with the experimental data and the decrease in the mobility at high effective normal field is interpreted in terms of surface-roughness scattering which results in E_{eff}^{-2} dependence at high normal fields.

KEYWORDS: n-Si MOSFET, inversion layer, effective normal field dependence, mobility

§1. Introduction

Mobility in semiconductors is one of the most important parameters of devices such as MOSFETs, bipolar transistors and HEMTs (high electron mobility transistors). Mobility reflects scattering mechanisms and electronic states of the carriers. In MOSFET structures, a strong gate field results in a confinement of carriers in a very thin channel layer below the gate and in the formation of two-dimensional electron gas (2DEG). In such a thin layer, therefore, quite different carrier transport behaivior is expected in contrast to the case of three-dimensional carriers in bulk materials. Since MOSFET conductance is proportional to carrier mobility, device characteristics are determined by the mobility. It is well known that GaAs MESFETs or HEMTs is superior for high-speed device application because of its high electron mobility compared with Si MOSFETs.

A number of field effect and Hall effect measurements have been carried out to investigate the dependence of carrier mobility in the Si surface inversion layer on normal electric field, temperature and crystal orientation.[1-5] In these earlier investigations, the observed anisotropy of the electron mobility is interpreted satisfactorily in terms of the effective mass anisotropy.[3] On the other hand, interpretation of the temperature and normal field dependence is not well established because of the complicated scattering mechanisms.

Kawaji[6] was the first to point out that the relaxation time of electrons in the Si inversion layer is proportional to the average width of the quantized states in the case of acoustic phonon scattering, where he assumed that 2DEG is scattered by surface localized phonons. He explained the electron sheet density dependences of mobility in terms of the change in the average width. Sakaki and Sugano[7] showed the validity of the 2DEG model for galvanomagnetic effects in the Si inversion layer. Although the effect of the confinement of electron gas, a 2DEG formation, has been clearly observed in the quantum Hall effect or the Shubnikov-de Haas effect at low temperatures, such an effect is not clearly seen at high temperatures due to the broadening of the density-of-state, but various experimental results are well explained when the quantization of the electrons is taken into account, as shown later.

From the view points of device modeling and simulation of MOSFETs, the evaluation of the effective mobility is very important because it determines the device characteristics. Various models are proposed for the electron mobility in Si inversion layers.[8-13] Shirahata and Hamaguchi[14] reported that the normal field dependence of the electron mobility is well explained in terms of quantization of electrons. Their analysis is based on the electron-phonon interaction model proposed by Price,[15] where they took into account the quantization by using the wave functions calculated self-consistently. However, this model cannot explain the strong normal field dependence reported by Takagi, Iwase and Toriumi,[5] where they interpreted the quadratic field dependence of the effective channel mobility in terms of the surface-roughness scattering. The importance of the surface-roughness scattering in Si inversion layers has been pointed out by Hartstein, Ning and Fowler[16] from the analysis of the sheet electron density dependence of the effective channel mobility. Quantitative analysis of their data has been made by Ando,[17] where he has shown that the calculated mobility with an interface roughness of 4.3 Å high and 15 Å long gives a good agreement with the observed mobility.

In this paper, we report the normal field dependence of the electron mobility in Si MOSFETs measured by the Hall effect and channel conductance methods at 77 K and

room temperature. We propose analytical expressions for the electron mobility in the Si inversion layer, where the quantization of the electrons is considered. We will show that these expressions properly include the anisotropy of effective mass, many valley structures, three kinds of g- and f-type intervalley phonons, acoustic phonon scattering and surface-roughness scattering. At low temperatures, impurity scattering plays an important role in determining mobility, and therefore, it is included in the analysis of the mobility at 77 K. In §2, we present experimental procedures and results. In §3, theoretical analysis of the electron mobility in Si inversion layers is given, and a comparison is made between the presented theory and experiments Finally, we summarize the present results in §4.

§2. Experiments and Results

The n-channel MOSFETs used in this study were fabricated on (100) Si wafers with the substrate doping density of 8×10^{16} cm^{-3}. The current channel was chosen along the ⟨110⟩ direction and its length L was 200 μm and its width W was 100 μm. The specimens had three pairs of voltage probes with an equal spacing of 50 μm on both sides of the channel. The gate oxide thickness T_{ox} was 25 nm.

Source-drain voltage V_d was kept at a constant value of 50 mV in the linear region for Hall effect measurements. A magnetic flux density of 0.15 T was applied perpendicular to the sample surface. Measurements were carried out at room temperature and liquid-nitrogen temperature.

Hall mobility, μ_H, and inversion layer electron density, N_s, were determined using the following relations:

$$\mu_H=(lV_H)/(WV_pB) \tag{2.1}$$

$$N_s=(I_dB)/(eV_H), \tag{2.2}$$

where V_H is the Hall voltage, V_p the voltage between the potential probes, I_d the drain current, l the length between potential probes, and e the magnitude of electronic charge.

Effective mobility μ_{eff} was also estimated from channel conductance measurements on the same sample, where we used a semiconductor parameter analyzer (YHP 4145B). The effective mobility is given by the following equations in the linear region.

$$\mu_{eff}=(LI_d)/(WV_deN_s'), \tag{2.3}$$

where V_d is drain voltage, and the inversion layer sheet electron density N_s' is given by

$$N_s'=C_{ox}(V_g-V_{th})/e. \tag{2.4}$$

In eq. (2.4), C_{ox} is the gate oxide capacitance per unit area, V_g is the gate voltage and V_{th} is the threshold voltage.

In Fig. 1 we plotted Hall mobility as a function of sheet electron density by open circles at 300 K and 77 K, along with effective mobility estimated from the channel conductance measurements by solid circles. We found a good agreement between the Hall and effective mobilities at 300 K, and hence we omitted the solid circles for the curve at 300 K. On the other hand, we found a noticeable discrepancy at 77 K between the two different measurements. The difference cannot be explained in terms of the scattering dependent coefficient γ_H (Hall factor), where the coefficient appears in the Hall coefficient R_H;

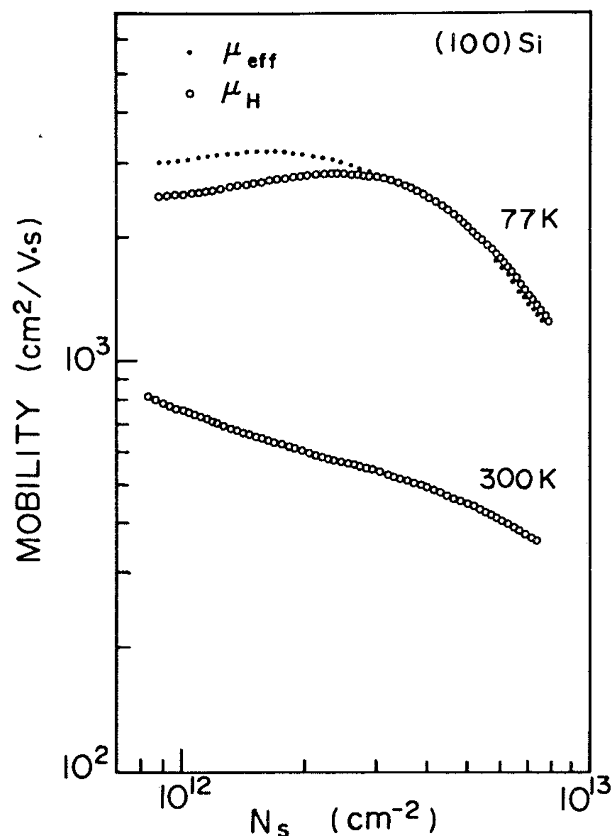

Fig. 1. Hall mobility (open circles) and effective channel mobility (closed circles) at 77 and 300 K as a function of sheet electron density in a (100) Si MOSFET sample with accepter density of 8×10^{16} cm^{-3}, gate width of 100 μm, length of 200 μm and oxide thickness of 250 Å.

$$R_H=\gamma_H/eN_s. \tag{2.5}$$

When we use the above equation, the Hall mobility is given by the drift mobility multiplied by the coefficient γ_H. It is well known that the Hall factor is 1.18 for acoustic phonon scattering and 1.93 for ionized impurity scattering.[18] Since ionized impurity scattering is dominant at lower temperatures, the Hall mobility is expected to be larger than the drift mobility at 77 K, which is in contrast to the present observation. We note that the Hall voltage at zero magnetic field vanishes, and thus we need no correction of the Hall voltage. In the present work, we made no correction due to the geometrical effects because the measured Hall mobility shows a good agreement with the effective mobility estimated from the FET characteristics except in the region of low sheet electron density.

It is also seen in Fig. 1 that the electron mobility at 300 K decreases monotonically with increasing inversion electron density. At 77 K, on the other hand, the electron mobility increases at first and then decreases at higher electron density. It is very interesting to point out that the electron mobility at 77 K decreases more steeply than at 300 K in the region of higher electron densities. This electron density dependence of electron mobility in the

region of high electron density will be interpreted by taking into account surface-roughness scattering.

It has been shown by Sabnis and Clemens[19] that the effective mobility can be expressed by a universal curve when it is plotted as a function of effective normal field which is defined by

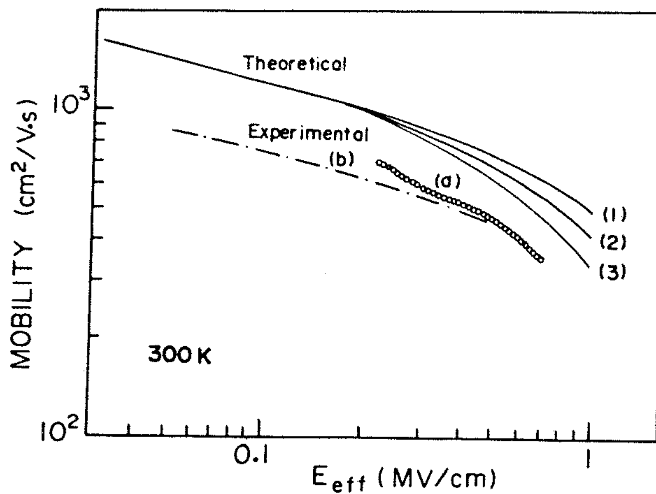

Fig. 2. The solid curves (1)–(3) are calculated using the surface-roughness parameters $\Delta\Lambda=20\times10^{-20}\,\mathrm{m}^2$ (1), $25\times10^{-20}\,\mathrm{m}^2$ (2) and $30\times10^{-20}\,\mathrm{m}^2$ (3), respectively. The present experimental data (Hall mobility) are shown by open circles (curve (a)) along with the experimental data of Cooper and Nelson (dot-dashed curve (b)) obtained by time-of-flight method. ($T=300$ K)

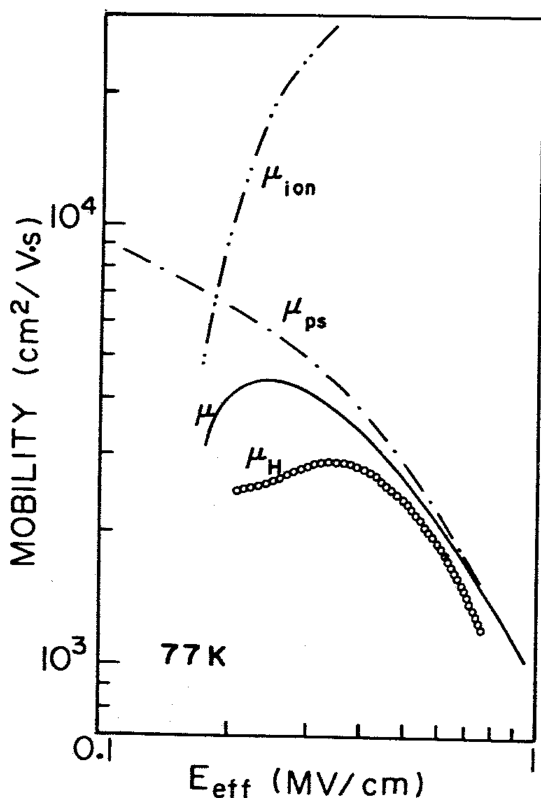

Fig. 3. Effective normal field dependence of the measured Hall mobility (open circles) is compared with the calculated mobility using the assumption described in the text. The dot-dashed curve (μ_{ps}) is calculated mobility due to acoustic phonons, intervalley phonons and surface-roughness scattering, while the double dot-dashed curve (μ_{ion}) is the calculated mobility due to the ionized impurity scattering alone. ($T=77$ K)

$$E_{\mathrm{eff}}=e(0.5N_{\mathrm{s}}+N_{\mathrm{depl}})/\kappa_{\mathrm{Si}}\varepsilon_0 \tag{2.6}$$

where N_{depl} is the charge density per unit area in the depletion layer, κ_{Si} the dielectric constant of Si and ε_0 the free-space permittivity.

The validity of the universal curve has been confirmed by Takagi, Iwase and Toriumi[5] very recently, where they measured the effective mobility in n- and p-channel MOSFETs with substrate impurity concentrations ranging from 10^{15} to $10^{18}\,\mathrm{cm}^{-3}$. We are concerned with the normal field dependence of the mobility analyzed by the model based on the 2DEG interacting with various phonon modes, impurities and surface-roughness in the next section, and therefore we present here the normal field dependence of the electron mobility estimated by using eq. (2.6) and the experimental data. Figures 2 and 3 represent the electron mobility as a function of normal effective field at 300 K and 77 K, respectively, where the open circles are the measured Hall mobility. The solid and dash-dotted curves will be described in detail in the next section. The present results are in good agreement with those of Takagi, Iwase and Toriumi.[5]

§3. Analysis and Discussion

The conduction band of bulk silicon has six valleys along the ⟨100⟩ directions of the Brillouin zone, and the constant energy surface is ellipsoidal with the transverse effective mass $m_t=0.19\,m_0$ and the longitudinal effective mass $m_l=0.92\,m_0$. In the (100) surface inversion layer, therefore, the six valleys are classified into two valleys with m_l perpendicular to the surface and four valleys with m_t perpendicular to the surface. It is well known that the electronic states in the inversion layer is quantized into subbands, the energies of which are proportional to $(m_3)^{1/3}$, where m_3 is the effective mass perpendicular to the surface.[20] The lowest energy subband arises from the two valleys with the perpendicular mass m_l and the higher-lying subband from the four valleys with the perpendicular mass m_t. We use Stern's notation,[20] E_i and $E_{i'}$, for the subband energies with $m_3=m_l$ and $m_3=m_t$, respectively. The electronic states of 2DEG are calculated by solving the Schrödinger equation and Poisson equation self-consistently

$$-\frac{\hbar^2}{2m_3}\frac{\mathrm{d}^2}{\mathrm{d}z^2}\xi_i(z)-e\phi(z)\xi_i(z)=E_i\xi_i(z), \tag{3.1}$$

$$\frac{\mathrm{d}^2\phi}{\mathrm{d}z^2}=-\frac{1}{\kappa_{\mathrm{Si}}\varepsilon_0}\left[\rho_{\mathrm{depl}}(z)-e\Sigma N_i\xi_i^2(z)\right] \tag{3.2}$$

where the notation is the same as that of Stern.[20] Numerically, calculations were carried out by a computer (HP9000 model 550) to obtain eigenvalues, envelope functions and subband sheet electron density as a function of normal field. As shown in Fig. 4 we found from the present calculations that more than 85% (90%) of the total electrons occupy the lower two subbands, E_0 and $E_{0'}$, in the region of high effective normal field at 300 K (at 77 K), and thus we took into account the electrons in these two subbands for calculating the mobility. This approximation was used by Shirahata and Hamaguchi[14] to analyze the normal field dependence of the electron mobility. However, we have to note here that their

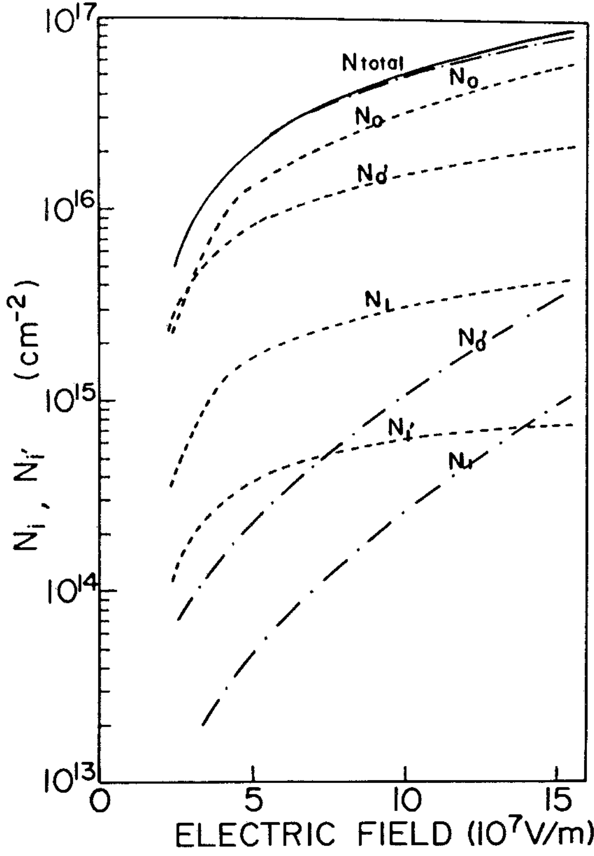

Fig. 4. Populations of electrons $N_{0(1)}$ and $N_{0(1)'}$ in the subbands $E_{0(1)}$ and $E_{0(1)'}$, respectively, in the (100) Si inversion layer with $N_A=8\times10^{16}$ cm^{-3} at 300 K (broken lines) and 77 K (dot-dashed lines). The solid line shows the total sheet density of electrons $N_{\rm total}$.

analysis is not quantitative, but adjustable parameters are used to fit the calculated curve with the experimental curve at a fixed point of the normal electric field.

It is well known from the analysis of hot-electron effects that the electrons in n-type silicon are scattered by various modes of phonons and that the intervalley phonon scattering dominates the other scattering processes, especially at high electric fields. Herring[21] and Long[22] have shown that the temperature dependence of the electron mobility is explained by considering the intervalley phonon scattering. Monte Carlo simulation of hot-electrons revealed that the electrons are scattered by g-type and f-type intervalley phonons and that the three intervalley phonon modes of g- and f-types are required to explain the hot electron transport[23] (See Fig. 5 for the g- and f-types of intervalley phonon scatterings). The deformation potentials for these intervalley phonon scatterings are determined from the Monte Carlo simulation which are tabulated in Table I, and other parameters used in the present analysis are shown in Table II. Since the density of states for 2DEG is characterized by a step function, as shown below, the electron mobility is analytically evaluated when we know the envelope function.

The relaxation time of the 2DEG interacting with three-dimensional phonons is derived by Price[15] and Ridley.[24] The scattering rate is proportional to

$$\int C^2(q)I_{mn}(q_z)^2\,{\rm d}q_z, \tag{3.3}$$

Table I. Set of intervalley phonon scattering parameters (Brunetti *et al.*[23])

Type of intervalley scattering	T (K)	D_j (10^8 eV/cm)
$f1$	220	0.3
$f2$	550	2.0
$f3$	685	2.0
$g1$	140	0.50
$g2$	215	0.80
$g3$	720	11.0

Table II. Set of physical parameters in the present calculations.

m_0	free electron mass	9.11×10^{-31} (kg)
m_l	longitudinal effective mass	$0.916\,m_0$
m_t	transverse effective mass	$0.19\,m_0$
m_d	density of state mass in subband E_0	$0.19\,m_0$
$m_{d'}$	density of state mass in subband $E_{0'}$	$0.417\,m_0$
ρ	crystal density	2,329 (kg/m^3)
s_l	sound velocity	9,037 (m/s)
$\kappa_{\rm Si}$	dielectric constant	11.7
$D_{\rm ac}$	acoustic deformation potential	12 (eV)

where $C(q)$ represents q dependence of the matrix element for electron-phonon interaction. In the present analysis, we assume that the electron-phonon interactions in the Si inversion layer is the same as those in bulk Si except for the quantization of electron wave functions, and we follow the treatment by Price[15] in which the matrix element of the electron-phonon interaction is characterized by the form factor

$$I_{mn}(q_z)=\int \xi_m^*(z)\xi_n(z)\exp({\rm i}q_z z)\,{\rm d}z, \tag{3.4}$$

where the phonon wave vector is $\vec{q}+\vec{q}_z$, and the momentum conservation is satisfied between the phonon wave vector $\vec{q}$ and electron wave vector $\vec{k}$ perpendicular to the quantization axis z. Under this assumption, we find that there exist g-type intervalley intrasubband transition for E_0 subbands and f- and g-types of intervalley intrasubband transitions for $E_{0'}$ subbands, while intersubband transition occurs only by the f-type intervalley scattering.

In the case of scattering by deformation potential acoustic phonons and intervalley phonons, eq. (3.3) reduces to

$$\int C^2 I_{mn}(q_z)^2\,{\rm d}q_z=C^2\int |I_{mn}(q_z)|^2\,{\rm d}q_z=\frac{\pi C^2}{b_{mn}}, \tag{3.5}$$

where

$$\frac{1}{b_{mn}}=2\int \zeta_m^2(z)\zeta_n^2(z)\,{\rm d}z. \tag{3.6}$$

These values are obtained by self-consistent calculations of the coupled Schrödinger and Poisson equations (3.1) and (3.2), which are reported by many authors.[20,25,26] The momentum-relaxation rates are given in the Appendix for deformation potential acoustic phonons, intervalley phonons, and surface-roughness scattering. Using these relaxation times, we are able to evaluate the electron mobility in the subbands E_0 and $E_{0'}$. However, the ex-

istence of the various intervalley phonon modes results in a very complicated form for the mobility. Therefore we present a simplified case, where the electron scattering is dominated by an acoustic phonon, surface-roughness, and one of the g-type and one of the f-type intervalley phonon scattering, and later, we evaluate the mobility including all the modes of the intervalley phonons.

Let us assume that electrons are scattered by acoustic phonons, interface roughness, the f-type intervalley phonons (fi) with the energy $\hbar\omega_{fi}$, and the g-type intervalley phonons (gi) with the energy $\hbar\omega_{gi}$. We have to note here that intersubband scattering should be included for both acoustic and intervalley phonon scatterings, but the intersubband scattering by the acoustic phonons is not allowed for the transition from the E_0 subband to the $E_{0'}$ subband because the involved acoustic phonon energy is much less than the energy separation between the two subbands.

Under the assumption stated above, we obtain the total scattering rate for the electrons in the subband E_0

$$\frac{1}{\tau_0}=(A_0+B_0)u(\varepsilon)+C_{0gi}[N_{gi}u(\varepsilon)+(N_{gi}+1)u(\varepsilon-\hbar\omega_{gi})]+4C_{0fi}[N_{fi}u(\varepsilon-\Delta\varepsilon+\hbar\omega_{fi})+(N_{fi}+1)u(\varepsilon-\Delta\varepsilon-\hbar\omega_{fi})], \quad (3.7)$$

and for the electrons in the subband $E_{0'}$

$$\frac{1}{\tau_{0'}}=(A_{0'}+B_{0'})u(\varepsilon)+C_{0'gi}[N_{gi}u(\varepsilon)+(N_{gi}+1)u(\varepsilon-\hbar\omega_{gi})]+2C_{0'fi}[N_{fi}u(\varepsilon)+(N_{fi}+1)u(\varepsilon-\hbar\omega_{fi})]+2C'_{0fi}[N_{fi}u(\varepsilon)+(N_{fi}+1)u(\varepsilon+\Delta\varepsilon-\hbar\omega_{fi})], \quad (3.8)$$

where

$$A_0=\frac{m_d D_{ac}^2 k_B T}{\hbar^3 \rho s_l^2}\frac{1}{2b_{00}}, \quad (3.9a)$$

$$B_0=\pi m_d(\Delta\Lambda e E_{eff})^2/\hbar^3, \quad (3.9b)$$

$$C_{0gi}=\frac{m_d D_{gi}^2}{2\hbar\rho\hbar\omega_{gi}}\frac{1}{b_{00}}, \quad (3.9c)$$

$$C_{0fi}=\frac{m_{d'} D_{fi}^2}{2\hbar\rho\hbar\omega_{fi}}\frac{1}{b_{00'}}, \quad (3.9d)$$

$$A_{0'}=\frac{m_{d'} D_{ac}^2 k_B T}{\hbar^3 \rho s_l^2}\frac{1}{2b_{0'0'}}, \quad (3.9e)$$

$$B_{0'}=\pi m_{d'}(\Delta\Lambda e E_{eff})^2/\hbar^3, \quad (3.9f)$$

$$C_{0'gi}=\frac{m_{d'} D_{gi}^2}{2\hbar\rho\hbar\omega_{gi}}\frac{1}{b_{0'0'}}, \quad (3.9g)$$

$$C_{0'fi}=\frac{m_{d'} D_{fi}^2}{2\hbar\rho\hbar\omega_{fi}}\frac{1}{b_{0'0'}}, \quad (3.9h)$$

$$C'_{0fi}=\frac{m_d D_{fi}^2}{2\hbar\rho\hbar\omega_{fi}}\frac{1}{b_{00'}}, \quad (3.9i)$$

$u(\varepsilon)$ is the unit step function ($u(\varepsilon)=0$ for $\varepsilon<0$ and $u(\varepsilon)=1$ for $\varepsilon\geq 0$) which arises from the density-of-state function of 2DEG, and $\Delta\varepsilon$ is the energy difference between the two subbands. In eq. (3.7), the factor 4 arises from valley degeneracy of the subband $E_{0'}$. Similarly, in eq. (3.8), the factor 2 is evident from the schematic drawing in Fig. 5.

The average of the relaxation time is easily evaluated when we assume Maxwellian distribution for the electrons and is given by

$$\langle\tau\rangle=\int\tau\varepsilon f_0\,d\varepsilon\bigg/\int\varepsilon f_0\,d\varepsilon. \quad (3.10)$$

When eq. (3.7) is inserted in the eq. (3.10) we obtain

$$\langle\tau_0\rangle=\frac{F(0,x_{gi})}{A_0+B_0+C_{0gi}N_{gi}}+\frac{F(x_{gi},x_0-x_{fi})}{A_0+B_0+C_{0gi}(2N_{gi}+1)}+\frac{F(x_0-x_{fi},x_0+x_{fi})}{A_0+B_0+C_{0gi}(2N_{gi}+1)+4C_{0fi}N_{fi}}+\frac{G(x_0+x_{fi})}{A_0+B_0+C_{0gi}(2N_{gi}+1)+4C_{0fi}(2N_{fi}+1)}, \quad (3.11)$$

where we introduce the following dimensionless quantities,

$$x_{gi}=\hbar\omega_{gi}/k_B T, \quad (3.12a)$$

$$x_{fi}=\hbar\omega_{fi}/k_B T, \quad (3.12b)$$

$$x_0=\Delta\varepsilon/k_B T=(E_{0'}-E_0)/k_B T, \quad (3.12c)$$

and the functions $F(x, y)$ and $G(x)$ are defined by

$$F(x,y)=\int_x^y x\exp(-x)\,dx=(1+x)\exp(-x)-(1+y)\exp(-y), \quad (3.13a)$$

$$G(x)=\int_x^\infty x\exp(-x)\,dx=(1+x)\exp(-x). \quad (3.13b)$$

In a similar fashion the averaged relaxation time in the $E_{0'}$ subband is given by

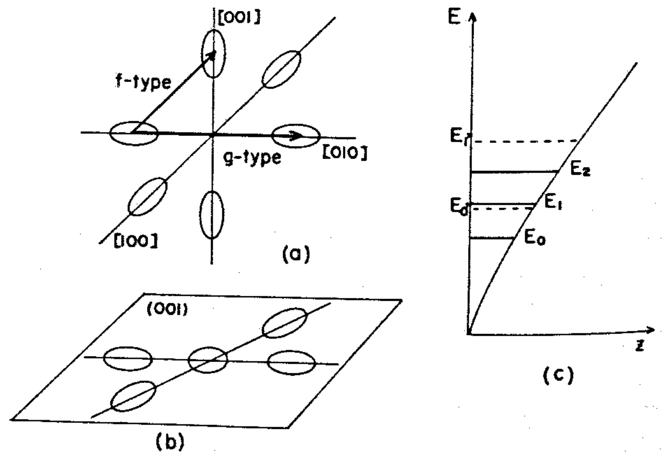

Fig. 5. Schematic representation of the constant energy ellipses of (a) bulk Si and (b) two-dimensional electron gas for the (001) Si surface. The subband energies are also shown in (c) schematically for a triangular potential case.

$$\langle\tau_{0'}\rangle=\frac{F(0,x_{gi})}{A_{0'}+B_{0'}+C_{0'gi}N_{gi}+2C_{0'fi}N_{fi}+2C'_{0fi}(2N_{fi}+1)}+\frac{F(x_{gi},x_{fi})}{A_{0'}+B_{0'}+C_{0'gi}(2N_{gi}+1)+2C_{0'fi}N_{fi}+2C'_{0fi}(2N_{fi}+1)}$$
$$+\frac{G(x_{fi})}{A_{0'}+B_{0'}+C_{0'gi}(2N_{gi}+1)+2C_{0'fi}(2N_{fi}+1)+2C'_{0fi}(2N_{fi}+1)}. \qquad (3.14)$$

Note that the right-hand sides of eqs. (3.11) and (3.14) are evaluated by considering the energy range of integration (in order of energy; $x_{gi}<x_{fi}<x_0$). The average mobility is defined as

$$\mu=\frac{(N_0e\langle\tau_0\rangle/m_c+N_{0'}e\langle\tau_{0'}\rangle/m_{c'})}{(N+N_{0'})}, \qquad (3.15)$$

where N_0 and $m_c(=m_t)$ are the sheet electron densities and the conductivity mass in the E_0 subband, respectively, and $N_{0'}$ and $m_{c'}(=2m_tm_l/(m_t+m_l))$ are those in subband $E_{0'}$.

It is straightforward to calculate the average relaxation times in the presence of three modes of intervalley phonons, and the averaged relaxation time for the E_0 subband is given by

$$\frac{1}{\tau_0}=(A_0+B_0)u(\varepsilon)+\sum_{i=1}^{3}C_{0gi}[N_{gi}u(\varepsilon)+(N_{gi}+1)u(\varepsilon-\hbar\omega_{gi})]+4\sum_{i=1}^{3}C_{0fi}[N_{fi}u(\varepsilon-\Delta\varepsilon+\hbar\omega_{fi})+(N_{fi}+1)u(\varepsilon-\Delta\varepsilon-\hbar\omega_{fi})], \qquad (3.16)$$

where the summation runs from the lowest-energy phonons to highest-energy phonons for both f- and g-type phonons, and the evaluation of the average mobility using eq. (3.10) should be carried out by dividing the integration range in order of energy. Similarly, the averaged relaxation time for the electrons in the $E_{0'}$ subband is given by

$$\frac{1}{\tau_{0'}}=(A_{0'}+B_{0'})u(\varepsilon)+\sum_{i=1}^{3}C_{0'gi}[N_{gi}u(\varepsilon)+(N_{gi}+1)u(\varepsilon-\hbar\omega_{gi})]+2\sum_{i=1}^{3}C_{0'fi}[N_{fi}u(\varepsilon)+(N_{fi}+1)u(\varepsilon-\hbar\omega_{fi})]+2\sum_{i=1}^{3}C'_{0fi}[N_{fi}u(\varepsilon)+(N_{fi}+1)u(\varepsilon+\Delta\varepsilon-\hbar\omega_{fi})]. \qquad (3.17)$$

Next, we will be concerned with the normal field dependence of the electron mobility, where the normal field depends on the sheet electron density in the inversion layer and their relation is given by eq. (2.6). The sheet electron density is easily evaluated from the channel conductance measurements when we know the geometry of the specimens and the thickness of the oxide layer. As stated in §2, we measured Hall voltage in the same samples and obtained the sheet electron density which was found to be in good agreement with the values estimated from the channel conductance measurements. Using these values and impurity concentrations in the substrate, we are able to obtain the sheet electron densities in the E_0 and $E_{0'}$ subbands from the self-consistent analysis. The self-consistent analysis also gives the subband energies and the envelope functions and thus the overlap integrals b_{mn}'s. Using these results, eqs. (3.16) and (3.17) are evaluated and the average mobility is obtained from eqs. (3.10) and (3.15).

The solid curves in Fig. 2 show the calculated results with three parameters of $\Delta\Lambda$ for surface-roughness scattering. The experimental data of Cooper and Nelson obtained by a time-of-flight method[13] is also shown in Fig. 2 to compare with the present results. The data of Cooper and Nelson exhibit a good agreement with the present experiments although the acceptor concentrations are different from each other, $N_A=1.2\times10^{14}\,\mathrm{cm}^{-3}$ for the sample used by Cooper and Nelson and $8.0\times10^{16}\,\mathrm{cm}^{-3}$ for our sample. This feature is consistent with the results that the effective mobilities measured in MOSFETs with different impurity concentrations lie on a universal curve at higher effective normal fields.[5] Although the calculated curves are found to be slightly higher than the experimental results, the effective normal field dependence of the mobilities calculated with $\Delta\Lambda$ ranging from 20 to $30\times10^{-20}\,\mathrm{m}^2$ is in good agreement with the experimental results. It is evident from the present analysis that the decrease in the mobility at high effective normal fields is caused by the surface-roughness scattering. The effective normal field dependence of the measured mobility is expressed by the relation $\mu\propto E_{\mathrm{eff}}^{-2}$.

Next we will deal with the analysis of the mobility at 77 K. As seen in Fig. 3, the electron mobility at 77 K decreases at lower effective normal fields, which may be interpreted in terms of impurity scattering. However, the treatment of the impurity scattering is complicated because of the screening effect, and the impurity scattering can only be evaluated by numerical calculation as shown below.

First, we will examine the scattering rate of 2DEG by impurity ions. The relaxation time for the impurity scattering of 2DEG from the state of the m-th subband with wave vector $\vec{k}_1$ to the state of the n-th subband with wave vector $\vec{k}_2$ due to the scattering by impurities in the substrate is given by,[27)*]

$$\frac{1}{\tau_{\mathrm{ion}}}=\frac{e^4m_d}{8\pi\hbar^3(\kappa_{\mathrm{Si}}\varepsilon_0)^2}\int_0^{2\pi}\frac{I_{mn}(q(\theta))(1-\cos\theta)}{[q(\theta)+PH_{mn}(q(\theta))]^2}\,\mathrm{d}\theta u(D), \qquad (3.18)$$

where $u(D)$ is the unit step function, P is the screening parameter and is given by

$$P=e^2N_s/(2\kappa_{\mathrm{Si}}\varepsilon_0k_BT), \qquad (3.19a)$$

$$H_{mn}(q(\theta))=\iint\zeta_m(z_1)\zeta_m(z_2)\zeta_n(z_1)\zeta_n(z_2)\times\exp\{-q(\theta)|z_1-z_2|\}\,\mathrm{d}z_1\,\mathrm{d}z_2, \qquad (3.19b)$$

*K. Miyatsuji: Master Thesis, Osaka University (1986).

$$I_{mn}(q(\theta))=\int N_d(z_0)\left[\int \zeta_n(z)\zeta_m(z)\times\exp\{-q(\theta)|z-z_0|\}\,dz\right]^2 dz_0, \tag{3.19c}$$

$$q(\theta)=|\vec{k}_1-\vec{k}_2|, \tag{3.19d}$$

$$D=k_1^2-2m_d(E_n-E_m)/\hbar^2, \tag{3.19e}$$

$N_d(z_0)$ is the impurity concentration in the direction of z, theta is the angle between the wave vectors $\vec{k}_1$ and $\vec{k}_2$, and E_m and E_n are the subband energies of the m-th and n-th subbands, respectively.

As we can see in eq. (3.18), the relaxation time for the impurity scattering is very complicated, and the evaluation of the average value cannot be made analytically, and therefore we adopt an approximation method as follows. First we evaluate the average relaxation time due to the impurity scattering by using numerical calculations, and then we combine the two average relaxation times using the formula

$$\frac{1}{\langle\tau_0\rangle}=\frac{1}{\langle\tau_{\rm ion}\rangle}+\frac{1}{\langle\tau_{\rm ps}\rangle} \tag{3.20}$$

for electrons in the E_0 subband, where $\langle\tau_{\rm ps}\rangle$ is the average relaxation time for scattering without the impurity scattering (scattering due to acoustic phonons, surface-roughness and intervalley phonons). The average relaxation time for electrons in the $E_{0'}$ subband is also calculated in the same manner. Then the average mobility is evaluated using eq. (3.15).

The solid curve in Fig. 3 is the calculated result with impurity concentration $8\times10^{16}\,\text{cm}^{-3}$ and roughness parameter $\Delta\Lambda=25\times10^{-20}\,\text{m}^2$, which shows a reasonable agreement with the present experiments. For the purpose of physical interpretation, we plotted the electron mobility limited by the impurity scattering by the double-dot-dashed curve and the mobility limited by phonon scattering and surface-roughness scattering by the dot-dashed curve. The increase in the mobility limited by the impurity scattering with increasing effective normal field is interpreted as the screening of the ionized impurity by the inversion electrons reducing the scattering rate at higher electron concentrations and thus at higher effective normal fields. It is very interesting to compare the results at 77 K with those at room temperature. We find that the effective normal field dependence of the mobility is approximated by $\mu\propto E_{\rm eff}^{-2}$. This feature is well explained in terms of the surface-roughness scattering. As seen in eq. (A·7) the relaxation time for the surface-roughness scattering is proportional to the square of the effective normal field. Although a reasonable agreement between the present experiments and the theory is obtained, the discrepancy at lower effective normal fields exists. However, we have to note here that our calculations are carried out using all the parameters determined in bulk Si, except the surface-roughness parameters. It is surprising to find that the experimental data are well interpreted by the present model in which the two-dimensional electron gas in the inversion layer is scattered by bulk phonons.

§4. Conclusion

Electron mobility in the Si inversion layer was determined as a function of gate voltage from the measurements of Hall effect and channel conductance at 300 and 77 K. The mobilities obtained by the two different methods showed a good agreement with each other. The effective normal field dependence of the mobility is in good agreement with the previously reported data.[4,5,13] In order to analyze the present data, we proposed a theoretical model for the electron mobility in the inversion layer, where we considered the quantization of electrons, electron-phonon interaction based on the Price model, surface-roughness scattering and screened ionized impurity scattering. In the analysis, only one adjustable parameter is used for the surface-roughness scattering and the other parameters, such as acoustic deformation potential and deformation potentials for the intervalley phonon scattering, are those determined from bulk Si. We used three different intervalley phonons for the g-type and f-type intervalley scatterings. We found that the electron mobility is expressed by an analytical formula in which all the scattering processes, except the impurity scattering, are taken into account. In the analysis, we need determine the wave functions and subband energies which are calculated by solving the coupled Schrödinger and Poisson equations self-consistently. The calculated curve shows a good agreement with the present observation in the magnitude of the mobility, and the effective normal field dependence of the mobility is well interpreted in terms of the surface-roughness scattering at higher gate fields. At 77 K, the electron mobility decreases in the region of low effective normal fields, which is explained by the impurity scattering and the screening effect. In the region of high effective normal field, the electron mobility decreases with increasing normal field as $E_{\rm eff}^{-2}$, which is well explained in terms of the surface-roughness scattering.

From the present work, we conclude that the electron mobility in Si inversion layers can be analyzed within the framework of the model proposed in this paper, where the two-dimensional electron gas is scattered by three-dimensional phonons, surface-roughness and screened ionized impurities.

Acknowledgments

One of the authors (K.M) thanks Professor S. Miyamoto and Professor M. Hamada, President, of Anan College of Technology for their encouragement and is also grateful to the Ministry of Education, Science and Culture for the visiting fellowship.

Appendix

The momentum-relaxation rates for deformation potential acoustic phonons, $\tau_{\rm ac}$, and for j-th mode of intervalley phonons, τ_j, are given by

$$\frac{1}{\tau_{\rm ac}}=\frac{m_d D_{\rm ac}^2 k_B T}{\hbar^3\rho s_l^2}\frac{1}{2b_{mn}}, \tag{A·1}$$

and

$$\frac{1}{\tau_j}=\frac{m_d D_j^2}{2h\rho h\omega_j}\frac{1}{b_{mn}}\left[N_j+\frac{1}{2}\pm\frac{1}{2}\right], \quad \text{(A·2)}$$

where plus and minus signs correspond to phonon emission and phonon absorption, respectively, $m_{d'}$ is effective density-of-state mass given by $m_d=m_t$ and $m_d=(m_t m_l)^{1/2}$ depending on the final subband states E_0 and $E_{0'}$, respectively, D_{ac} is the deformation potential for acoustic-phonon scattering, $\hbar$ is the Planck constant divided by 2π, ρ is the crystal density, s_l is the sound velocity, k_B is the Boltzmann constant, D_j is the deformation potential for j-th intervalley phonon scattering ($j=f1, f2, f3, g1, g2, g3$; three modes of f-type intervalley phonons and three modes of g-type intervalley phonons) and N_j is the occupation number of j-th intervalley phonons with the angular frequency ω_j given by

$$N_j=1/[\exp(\hbar\omega_j/k_B T)-1]. \quad \text{(A·3)}$$

The momentum relaxation time for interface roughness scattering is given by[28]

$$\frac{1}{\tau_{SR}}=\frac{2\pi}{\hbar}\sum_q[\Delta\Lambda eE_{eff}/\varepsilon(q)]^2[\exp(-q^2\Lambda^2/4)]\times(1-\cos\theta)\delta(\varepsilon_k-\varepsilon_{k-q}), \quad \text{(A·4)}$$

where E_{eff} is the effective normal field given by eq. (2.6), Δ the root mean square deviation of the interface, Λ the correlation length, $\vec{q}=\vec{k}'-\vec{k}$, $\vec{k}$ the initial wave vector of an electron, $\vec{k}'$ the final wave vector of the electron, θ the angle between $\vec{k}$ and $\vec{k}'$ and $\varepsilon(q)$ is the dielectric function with screening effect given by

$$\varepsilon(q)=1+\frac{e^2}{2\kappa_{Si}\varepsilon_0}\frac{1}{q}\frac{2m_d}{2\pi\hbar^2}F(q), \quad \text{(A·5)}$$

where

$$F(q)=\int dz\int dz'|\zeta(z)|^2|\zeta(z')|^2\exp(-q|z-z'|). \quad \text{(A·6)}$$

In the present analysis we neglect the screening effect and thus equation (A·4) reduces to

$$\frac{1}{\tau_{SR}}=\frac{2\pi}{\hbar}\sum_q[\Delta\Lambda eE_{eff}]^2[\exp(-q^2\Lambda^2/4)]\times(1-\cos\theta)\delta(\varepsilon_k-\varepsilon_{k-q}). \quad \text{(A·7)}$$

As shown by Hartstein *et al.*[16] the correlation length Λ is about 6 Å and the term $(1-\cos\theta)k^2\Lambda^2/2$ is much less than unity. In this case, the relaxation time for the interface roughness scattering is approximated by

$$\frac{1}{\tau_{SR}}=\pi m_d[\Delta\Lambda eE_{eff}]^2/\hbar^3. \quad \text{(A·8)}$$

References

1) F. F. Fang and A. B. Fowler: Phys. Rev. **169** (1968) 619.
2) N. St. Murphy, F. Berz and I. Flinn: Solid-State Electron. **12** (1969) 775.
3) T. Sato, Y. Takeishi, H. Hara and Y. Okamoto: Phys. Rev. B **4** (1971) 1950.
4) S. C. Sun and J. D. Plummer: IEEE Trans. Electron Devices **ED-27** (1980) 1497.
5) S. Takagi, M. Iwase and A. Toriumi: Int. Electron Device Meet. Technical Digest, (IEEE, New York, 1988) 398.
6) S. Kawaji: J. Phys. Soc. Jpn. **27** (1969) 906.
7) H. Sakaki and T. Sugano: Jpn. J. Appl. Phys. **10** (1971) 1016.
8) D. L. Scharfetter and H. K. Gummel: IEEE Trans. Electron Devices **ED-16** (1969) 64.
9) K. K. Thornber: J. Appl. Phys. **51** (1980) 2127.
10) K. Yamaguchi: IEEE Trans. Electron Devices **ED-30** (1983) 658.
11) M. S. Lin: IEEE Trans. Electron Devices **ED-32** (1985) 700.
12) S. A. Schwarz and S. E. Russek: IEEE Trans. Electron Devices **ED-30** (1983) 1634.
13) J. A. Cooper, Jr. and D. F. Nelson: J. Appl. Phys. **54** (1983) 1445.
14) M. Shirahata and C. Hamaguchi: Jpn. J. Appl. Phys. **25** (1986) 1040.
15) P. J. Price: Ann. Phys. **133** (1981) 217.
16) A. Hartstein, T. H. Ning and A. B. Fowler: Surf. Sci. **58** (1976) 178.
17) T. Ando: J. Phys. Soc. Jpn. **43** (1977) 1616.
18) K. Seeger: *Semiconductor Physics* (Springer-Verlag, Wien, 1973).
19) A. G. Sabnis and J. T. Clemens: Int. Electron Device Meet. Technical Digest (IEEE, New York, 1979) 18.
20) F. Stern: Phys. Rev. B **5** (1972) 4891.
21) C. Herring: Bell Syst. Tch. **34** (1955) 237.
22) D. Long: Phys. Rev. **120** (1960) 2024.
23) R. Brunetti, C. Jacoboni, F. Nava, L. Reggiani, G. Bosman and J. J. Zijlstra: J. Appl. Phys. **52** (1981) 6713.
24) B. K. Ridley: J. Phys. C **15** (1982) 5899.
25) K. Miyatsuji, H. Hihara and C. Hamaguchi: Superlattices & Microstructure **1** (1985) 43.
26) H. Hihara and C. Hamaguchi: Solid State Commun. **54** (1985) 485.
27) P. J. Price: Surf. Sci. **113** (1982) 199.
28) T. Ando, A. B. Fowler and F. Stern: Rev. Mod. Phys. **54** (1982) 437.